Generalized Traveling-Wave-Based Waveform Approximation Technique for the Efficient Signal Integrity Verification of Multicoupled Transmission Line System

Yungseon Eo, Seongkyun Shin, William R. Eisenstadt, and Jongin Shim

***Abstract*—As very large scale integration (VLSI) circuit speed rapidly increases, the inductive effects of interconnect lines strongly impact the signal integrity of a circuit. Since these inductive effects make the signal integrity problems much more serious as well as intricate, they become one of the critical issues in today's high-speed/high-density VLSI circuit design. In this paper, a generalized traveling-wave-based waveform approximation (TWA) technique is presented which can be accurately as well as efficiently employed for the signal integrity verification of the inductively dominated (moderate Q) multicoupled RLC transmission line system. The technique is composed of three steps. First, the signals in the multicoupled (n-coupled) transmission line system are decoupled into n-isolated eigen-modes (i.e., basis vectors). Next, the slow-transient low-frequency characteristics of the system response are determined, approximately, in the frequency-domain by using the dominant poles of the basis vectors. Finally, the fast-transient high-frequency characteristics of the system response are calculated in the time domain by using the traveling wave characteristics of the basis vectors. It is shown that the time-domain responses of the multicoupled RLC transmission line system can be accurately as well as efficiently modeled with the generalized TWA technique. Then, in inductance-dominant multicoupled interconnect networks, switching-dependent signal integrity, i.e., signal delay, crosstalk, ringing, and glitches are investigated extensively with the proposed technique.**

***Index Terms*—Crosstalk, delay, modal analysis, signal integrity, system pole, transmission line, traveling wave, VLSI interconnects.**

I. Introduction

Today's very large scale integration (VLSI) circuits integrate myriad logic gates into a single silicon chip and their operating clock speeds already exceed several gigahertz. The high level of the integration of VLSI circuits gives rise to serious signal integrity problems due to the interconnect lines. Longer interconnect lines lead to significant timing uncertainty and tighter spacing between the lines causing more substantial electromagnetic coupling, i.e., crosstalk [1], [2]. Further, the electrical lengths of interconnect lines become a significant fraction of the transient signal's fundamental and harmonic frequency wavelength. Including transmission line effects becomes important in order to improve simulation accuracy [3], [4]. What is worse, the inductive effects of the interconnect lines become more prominent as the circuit speed increases [4]–[6]. Inductive effects make the signal integrity problems much more serious as well as intricate. Thus, future VLSI system designers may be victims of unexpectedly complicated signal integrity problems due to the inductance-dominant transmission lines.

Signal integrity degradation of the VLSI system due to the interconnect lines is strongly correlated with the layout configurations, the circuit switching conditions, and termination conditions [7]. Moreover, the generic interconnect networks are too complicated to efficiently verify the signal integrity of the complicated VLSI interconnect network. Thus, the interconnect system has been, in general, modeled as a multicoupled transmission line system [3], [8]–[17] which includes nonlinear devices and frequency-dependent transmission line parameters. However, there is a generic conflict in the modeling between the driver characteristics and interconnect characteristics [3]. That is, time-dependent nonlinear device characteristics can be well characterized in the time domain while frequency-dependent transmission line characteristics are best characterized in the frequency domain. In order to accurately investigate the transmission line characteristics including the nonlinear or frequency-dependent characteristics, the system response has to be calculated at every frequency step or time step.

To this date, many clever techniques concerned with the signal transient analysis of the general multicoupled transmission line system have been developed. Basically, there have been four representative techniques to characterize the general multicoupled transmission line systems: (1) a SPICE-like circuit segment-model [18], which requires a huge computation time due to extra nodes and branches; (2) convolution techniques [16], [17], which also need huge computation time due to numerical integration; (3) state-based approach [12]; and (4) waveform relaxation techniques [13]–[15], which are more efficient in computation time than the first two techniques. However, it is known that the last two approaches may not be suitable to handle fast-varying signals [3]. Although a recursive convolution algorithm [3] or improved waveform relaxation techniques [13]–[15] can improve the computation time, it may not be fast enough for today's IC CAD tools since it still includes numerical integration algorithms. Traditional numerical integration algorithms (very accurate) may not be practical and not efficient enough for the signal integrity verification of complicated VLSI circuits, since they require huge amounts of computation time. Fast transient-signal analysis algorithms and closed-form models which preserve the accuracy within allowable bounds are highly desirable for efficient signal integrity verification. Clearly, there exists a tradeoff between accurate simulation and fast simulation.

In order to avoid computationally inefficient numerical integration, by assuming linear device models and frequency-independent transmission line parameters, many model order reduction techniques such as asymptotic waveform evaluation (AWE) or similar rational-function-based model order reduction techniques were developed [19]–[27]. Note, the linear device and constant transmission line approach that are assumed in the fast simulation algorithms can be considered to be conservative assumptions for signal integrity verification owing to the following reasons. First, wire resistance remains constant for moderate frequencies although skin effect increases the resistance at very high frequency. In general, the skin effect tends to suppress signal spikes (which have very high-frequency components). Second, since the inductance for a wire is reduced at high frequency, inductive effects are overestimated for high-frequency components. Third, nonlinear devices can have larger output impedance (inverse of slope of the I-V output curve) as input signal increases. That means the sharp input edge rate becomes blunt a bit [27]. Thus, nonlinear crosstalk tends to be smaller than that estimated with linear device assumption.

Previously reported fast-simulation techniques are, in general, very powerful for the timing verification of RC-dominant integrated circuit interconnect networks. However, they may not be stable or computationally efficient for fast-transient signal simulations of the inductance-dominant multicoupled transmission line system [5]. Further, it is inherently very difficult to find the closed-form solution for timing and noise models with these techniques. Recently, Ismail

Manuscript received February 1, 2002; revised April 23, 2002. This work was supported in part by the Center for Electronic Packaging Material, Korea Science and Engineering Foundation. This paper was recommended by Associate Editor W. Schoenmaker.

Y. Eo, S. Shin, and J. Shim are with the Department of Electrical and Computer Engineering, Hanyang University, Ansan, 425-791, South Korea (e-mail: eo@giga.hanyang.ac.kr; ssk@giga.hanyang.ac.kr; jishim@giga.hanyang.ac.kr).

W. R. Eisenstadt is with the Department of Electrical and Computer Engineering, University of Florida, Gainesville, FL 32603 USA (e-mail: wre@tec.ufl.edu).

Digital Object Identifier 10.1109/TCAD.2002.804381

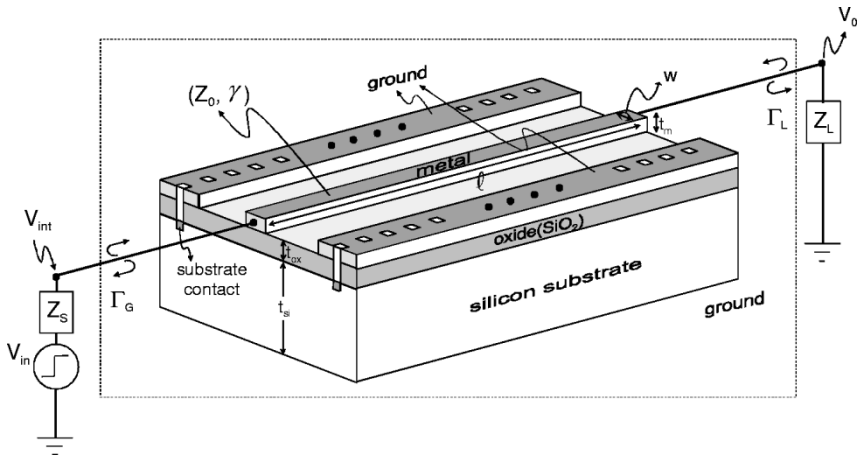

Fig. 1. Schematic circuit diagram of a transmission line with characteristic impedance $\boldsymbol{Z}_0$ and propagation constant $\boldsymbol{\gamma}$.

et al. developed a very good timing model which can be usefully employed for resistance/inductance/capatance (RLC) tree structure interconnect networks [28]. However, it may not be employed for the strongly coupled RLC-line system. Cao *et al.* derived an analytical timing model by mathematically collapsing two-coupled RLC lines into an effective isolated line [29]. However, this technique is not general since it is not suitable for the multicoupled lines with more than two lines. Davis and Meindl derived the time-domain responses in analytical manner for the limited cases of two- and triple-coupled lines based on the modified Bessel function [30]. Although the model is accurate for the intended applications, it is too complicated to be extended to general multicoupled lines with more than three-coupled lines. Yin and He developed a computationally efficient decoupling technique for two-coupled lines using a modal analysis technique [31]. Then, the time-domain transient-response signals for the isolated lines were determined with a conventional dominant pole approximation technique (i.e., rational function approximation). However, this may not be stable in inductance-dominant lines. Note, unlike the interline capacitive coupling, the inductive coupling may have a substantial effect on distant line characteristics within the system. The signal integrity of the high-speed/high-density VLSI circuits should be guaranteed in more than three-coupled adjacent lines for inductive coupling. Thus, they need to be extended into the general n-coupled transmission line system. Recently, Eo *et al.* developed a novel signal transient characterization technique for a single transmission line which is named traveling-wave-based waveform approximation (TWA) technique [32]. In the original work, the physical phenomena of the transient signal of a transmission line were characterized by combining the frequency-domain approximation technique for slow-transient characteristics and the time-domain approximation technique for fast-transient characteristics of the system response. In the frequency-domain, the transient signal is represented with only three-dominant poles which can represent, fairly accurately, its low-frequency characteristics. In contrast, the high-frequency characteristics of the transient signal are represented with the traveling wave characteristics and a modified-RC-response approximation technique in the time-domain. This enables the derivation of the accurate signal transient waveforms as well as analytic delay models for an inductance-dominant RLC interconnect line. The TWA technique is in the category of the fast simulation methodologies. That is, the technique focuses on a fast simulation within a tolerable accuracy under the assumption that loads and sources are linear and transmission line parameters are frequency independent. Thereby, the computation time can be significantly reduced (more than several thousand times compared to slow methodologies) in signal integrity simulation. With the original TWA-technique paper, it was shown that the technique is very accurately as well as efficiently employed for a single isolated line with approximately 5% error or less. However, since the original TWA technique [32] is focused only on the timing verification of a single isolated line, the signal integrity such as coupling effects (i.e., crosstalk) and switching-pattern-dependency effects due to multiple lines could not be investigated.

In this work, the original TWA technique is generalized for the signal integrity verification (i.e., delay, crosstalk, glitch, ringing, and switching-dependency) of multicoupled RLC transmission line systems, taking all the aforementioned effects into account. Then, it is shown that the signal integrity of the multicoupled interconnect lines can be readily investigated with this generalized TWA-technique. The details of the algorithm are discussed in the ensuing sections.

II. Signal Transient Characterization With TWA Technique

The incident power of a transmitted signal in a distributed circuit is not completely consumed in a load without an impedance match as in the case of high-speed CMOS circuits. When the load does not absorb power, the undissipated power is reflected back toward the source. The reflection of the incident wave occurs momentarily in the impedance discontinuity (i.e., $Z_o \neq Z_L$). The output waveform ($v_o(t)$) of the circuit of Fig. 1 changes abruptly with the discontinuity. That clearly implies the system has high-frequency eigenvalues (i.e., poles) which are associated with the system energy spectrum. Thus, the time-domain responses of the interconnect lines definitely include low-frequency eigenvalues as well as high-frequency eigenvalues. In the TWA, the low-frequency characteristics are modeled in the frequency-domain with three-pole approximation technique. In contrast, the fast-varying transients are modeled by exploiting the time-domain traveling-wave characteristics without resorting to the high-frequency poles. Thereby, the complete analytical time-domain responses are accurately determined [32].

In the frequency-domain, the system function of a single transmission line with a capacitive load is represented by [33], [34]

$$H(s,x) = \frac{Z_o}{Z_o + Z_s} \frac{\exp(-\gamma x) - \rho_l \exp(\gamma(2\ell - x))}{1 - \rho_s \rho_l \exp(-2\gamma\ell)} \tag{1}$$

where $\rho_s = (Z_s - Z_o)/(Z_s + Z_o)$, $\rho_l = (Z_L - Z_o)/(Z_L + Z_o)$, $\gamma = \sqrt{(R + sL)\,sC}$, $Z_0 = \sqrt{(R + sL)/sC}$, $Z_L = 1/(sC_L)$. Unlike timing verification, crosstalk noises may be substantial at both the

near end and the far end. Thus, the transfer function has to be separately modeled in the far end and near end as follows:

$$\begin{aligned} H(s, x=l) &\equiv H_{\text{far}}(s) \\ &= \frac{1}{\left(1+\frac{Z_S}{Z_L}\right)\cosh(\gamma\ell)+\left(\frac{Z_S}{Z_0}+\frac{Z_0}{Z_L}\right)\sinh(\gamma\ell)} \end{aligned} \tag{2}$$

$$\begin{aligned} H(s, x=0) &\equiv H_{\text{near}}(s) \\ &= \frac{Z_0 Z_L \cosh(\gamma\ell)+Z_0^2\sinh(\gamma\ell)}{Z_0(Z_S+Z_L)\cosh(\gamma\ell)+(Z_0^2+Z_S Z_L)\sinh(\gamma\ell)}. \end{aligned} \tag{3}$$

Note, it is not efficient to directly transform these frequency domain functions into the time domain since that requires time-consuming numerical integration. In order to overcome this problem, the Pade approximation technique has been frequently employed in investigations. However, Pade-based multipole approximation techniques may not be stable in inductance-dominant lines [5]. Note, a reflecting traveling wave (the overall wave can become a staircase of increasing or of decreasing step pulses passing a point) experiences a fast-time-varying transient when it reflects from a discontinuity. In contrast, until the next reflection, it is slowly transient toward a steady state. In the TWA technique, the slow-transient characteristics are approximated in the frequency domain with a finite number of poles and the fast-transient characteristics are incorporated in the time domain by utilizing the traveling wave characteristics and an RC-response-like waveform approximation technique.

In the frequency domain, although the two-pole approximation may be accurate enough for a capacitance-dominated system, it is not really sufficient for an RLC transmission line with moderate inductance. On the contrary, it is very difficult to solve the more than a third-order equation in an analytical manner. Therefore, the frequency domain system functions are approximated with three poles. With the first three dominant poles, the far-end system function is approximated by

$$\begin{aligned} H_{\text{far}}(s) &\approx \frac{1}{1+b_1 s+b_2 s^2+b_3 s^3} \\ &= \frac{1}{b_3(s-s_1)(s-s_2)(s-s_3)} \end{aligned} \tag{4}$$

where b_i is a constant. Similarly in the near end, the approximated transfer function is given by

$$\begin{aligned} H_{\text{near}}(s) &\approx \frac{q_1+q_2 s+q_3 s^2+q_4 s^3}{p_1+p_2 s+p_3 s^2+p_4 s^3} \\ &= \frac{q_4}{p_4}+\frac{\left(q_1-\frac{p_1}{p_4}q_4\right)+\left(q_2-\frac{p_2}{p_4}q_4\right)s+\left(q_3-\frac{p_3}{p_4}q_4\right)s^2}{p_4(s-s_1)(s-s_2)(s-s_3)} \end{aligned} \tag{5}$$

where p_i and q_i are constants. The coefficients b_i and p_i can be determined by Taylor series expansion. The system poles can be determined by solving the third-order polynomial equation in an analytical manner. The coefficients q_i can be readily determined by using the residue theorem. Then, the three-pole-approximation-based frequency-domain response of the system (i.e., $V_{03}(s)$: the subscript indicates the 3-pole-based output response) which does not include the high-frequency characteristics (i.e., high-frequency poles) can be determined as

$$V_{03}(s) \approx V_{in}(s) \cdot H(s). \tag{6}$$

Thus, the time-domain step response of the system

$$v_{03}(t) \approx \Im^{-1}\left\{\frac{1}{s}\cdot H(s)\right\} \tag{7}$$

can be directly determined without any integral calculation. Note that (7) does not incorporate the high-frequency characteristics (i.e., fast-transient characteristics) which will be considered in the time-domain. That is, the high-frequency characteristics of the transient signal are incorporated into the approximation function by utilizing the traveling wave characteristics and a modified-RC-response approximation technique in the time domain as follows. Right before the first incident wave arrives at the load, the time of the flight of a wave is given by $t_f^- \approx \sqrt{L_{\text{line}}C_{\text{line}}}$. Including the load capacitance C_L, an effective time of flight (t_{f0}) is approximately $t_{f0} \approx \sqrt{L_{\text{line}}(C_{\text{line}}+C_L)}$. The instant right before an incident wave is reflected can be represented by $t_f^- = t_{fo} - \delta$ and the instant right after an incident wave is reflected at the load can be represented by $t_f^+ = t_{fo} + \delta$. Note, the superscripts, "$-$" and "$+$" denote "right before" and "right after," respectively. The quantity δ is defined as

$$\delta \equiv \sqrt{L_{\text{line}}(C_{\text{line}}+C_L)} - \sqrt{L_{\text{line}}C_{\text{line}}}. \tag{8}$$

The δ denotes the time difference between the flight time of the pure (unloaded) line and that of the line including the loading effect. It can be assumed that the signal with multiple reflections will reach the load at roughly $(2n-1)t_{fo} - \delta$, where $n = 1, 2, 3, \ldots$ (note, n is the reflection count). Thus, until $t = t_f^-$, there exists no reflection due to the load discontinuity. Note, a traveling wave (consider a step pulse) can be considered to include all the frequency components from dc to very high frequency. Most of the low frequency components will be reflected at the capacitive load (CMOS gate) since the magnitude of load reflection coefficient for the low frequency components is approximately one. Thus, the low-frequency spectral components which contain the major part of the signal energy may experience a fast-transient discontinuity due to the reflection in the time interval between $(2n-1)t_{f0} - \delta$ and $(2n-1)t_{f0} + \delta$. In this abrupt transient time interval, the signal waveform can be approximated with a linear function. In contrast, a portion of the high frequency components is likely to be absorbed at the capacitive load, while the remaining portion of the high-frequency components is reflected. The result is the sharp edge part of a transient pulse may become blunt, thereby making the output similar to an RC-response-like wave shape. Thus, in the time interval between $(2n-1)t_{f0} + \delta$ and $(2n+1)t_{f0} - \delta$, the waveform can be modeled approximately with the RC-response-like approximation function. The time constant for the fictitious charging or discharging can be approximated by using the effective RC time constant (including C_L) of the system. The fictitious charging or discharging time constant τ can be reasonably approximated as $\tau \approx R_{\text{line}}(C_{\text{line}}+C_L)$. In summary, the TWA technique for a single line is composed of two steps, the three-pole approximation for the slow-transient characteristics in the frequency-domain and traveling-wave-based waveform approximation for the fast-transient characteristics in the time-domain. However, the single-line-based technique cannot be directly applied for the multiple lines since the multiple lines are electromagnetically coupled. The generalized TWA technique for the multicoupled lines will be presented in more detail in the next section.

III. Generalization of the TWA Technique for Multicoupled Transmission Line System

The n-coupled transmission line system can be modeled as a matrix form of Telegrapher equations [8]–[17]. In the frequency-domain, the Telegrapher equations are

$$\frac{d[V(x)]}{dx} = [Z][I(x)] \tag{9}$$

$$\frac{d[I(x)]}{dx} = [Y][V(x)] \tag{10}$$

where $[Z]$ and $[Y]$ are the series impedance matrix ($n \times n$ matrix) and parallel admittance matrix ($n \times n$ matrix) of the system, respectively. They are represented with per-unit-length transmission line parameters, i.e., $[Z] = [R] + s[L]$ and $[Y] = [G] + s[C]$. $[R]$, $[L]$, $[G]$, and $[C]$ are per-unit-length (PUL) transmission line circuit parameter matrices, i.e., PUL-resistance matrix, PUL-inductance matrix, PUL-conductance matrix, and PUL-capacitance matrix. Note that all these matrices are symmetric. As shown in (9) and (10), the response signals in a multicoupled line system are entangled in a complicated fashion with the coupling signals due to the interactions between the lines. Thus, it is too difficult to directly investigate the signal variations.

It is well known that n-coupled transmission lines can be decoupled into n-isolated lines by using the modal analysis technique [8]–[11], [31]. Then, the time-domain responses of the multicoupled lines are represented by the linear combination of the time-domain responses of the isolated modal basis vectors. The time-domain responses of the multicoupled lines can be accurately and efficiently determined with the TWA technique as in the single isolated line if the multicoupled line responses are decoupled into the eigenmodes. Note, since all the transmission line parameters are constant, the system matrix $[Z][Y]$ for a physically meaningful system is always diagonalizable [3], the eigenvalues and eigenmatrix can be readily determined by performing a similarity transform. Once they are determined, the frequency domain response function for each mode can be estimated by using a three-pole approximation technique. Then by separating the frequency domain approximation function of each mode into the partial fractional form, the time domain counter part of the frequency domain approximation function can be determined without any integral calculation. However, the time domain counterpart is not the complete waveform since the high-frequency characteristics are not considered yet. Thus, in next step, the fast-transient high-frequency characteristics are considered in the time domain by using the traveling wave-characteristics and a modified RC-approximation technique. Then, the final time-domain waveforms can be determined by the linear combination of each mode.

In order to decouple the voltage signal variations of the multicoupled lines into the isolated modal basis vectors of the system, the system is represented only with the voltage vector by combining (9) and (10)

$$\frac{d^2[V(x)]}{dx^2} = [Z][Y][V(x)]. \tag{11}$$

Then, the eigenvalue equation of the system can be obtained. If the system is composed of n-coupled lines, the system matrix is $n \times n$ matrix. Thus, the system has n-eigenvalues and $n \times n$ eigenmatrix. The eigenvalues, i.e., γ_i^2 ($i = 1, 2, \ldots, n$) are associated with the eigenpropagation modes of the system. Denoting the normalized voltage eigenvector as $[S]_n$, the diagonal matrix $[\Gamma]$ associated with the eigenvalues is given by

$$[\Gamma] = [Z_m][Y_m] = \begin{bmatrix} \gamma_1^2 & \cdots & 0 \\ \vdots & \ddots & \vdots \\ 0 & \cdots & \gamma_n^2 \end{bmatrix} \tag{12}$$

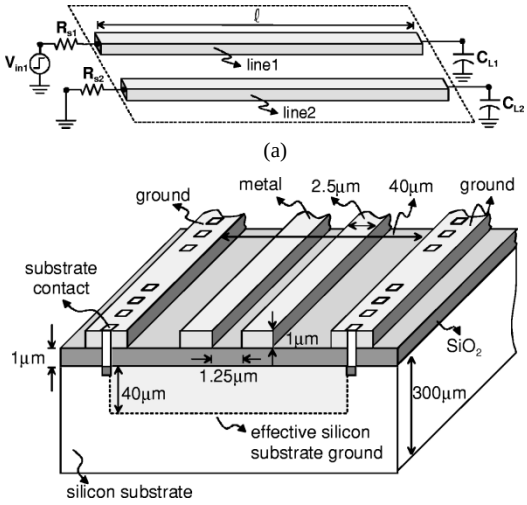

Fig. 2. Two-coupled transmission line system: (a) circuit diagram and (b) cross section.

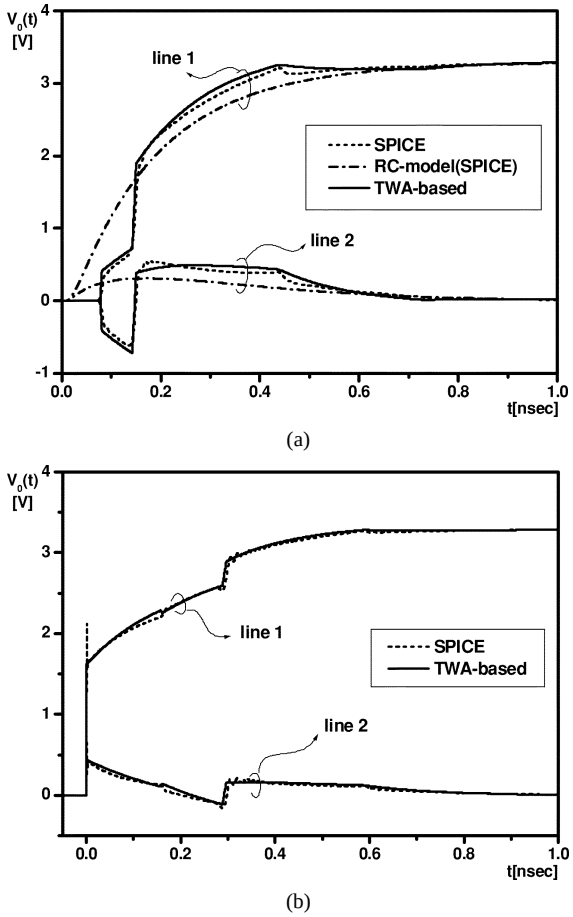

Fig. 3. Transient characteristics in two-coupled line system. The 3.3-V step input is applied to the line–1. All the source resistances are assumed to be $\boldsymbol{R}_{S1} = \boldsymbol{R}_{S2} = 50\,\Omega$. All the load capacitances are assumed to be $\boldsymbol{C}_{L1} = \boldsymbol{C}_{L2} = 0.1$ pF. (a) Waveforms at far end. (b) Waveforms at near end.

where $[Z_m]$ and $[Y_m]$ are modal impedance and modal admittance, respectively

$$[Z_m] = [R_m] + s[L_m] \tag{13}$$

$$[Y_m] = [G_m] + s[C_m]. \tag{14}$$

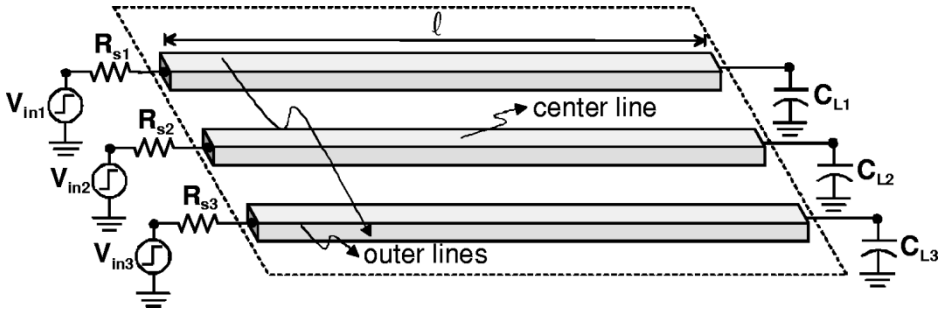

Fig. 4. Three-coupled transmission line system.

The modal transmission line parameters of the system are calculated as [35]

$$[R_m] = [S]_n^{-1}[R]\left([S]_n^{-1}\right)^T \quad (15)$$

$$[L_m] = [S]_n^{-1}[L]\left([S]_n^{-1}\right)^T \quad (16)$$

$$[C_m] = [S]_n^T[C][S]_n \quad (17)$$

$$[G_m] = [S]_n^T[G][S]_n . \quad (18)$$

Thus, the voltage equation can be decoupled with the modal basis (i.e., eigenvectors) of the system

$$[V(x)] = [S]_n\left([E(x)][B_1] - [E(x)]^{-1}[B_2]\right) \quad (19)$$

where $[E(x)] = \mathrm{diag}\left(e^{-r_i x}\right)$ is an $n \times n$ diagonal eigenmode matrix. The constant vectors (i.e., $[B_1]$ and $[B_2]$) can be completely determined with the boundary conditions. Note that physically the first term of the right-hand side of (19) is concerned with the incident waves and the second term on the right-hand side of (19) is concerned with the reflected waves. Now, since the voltage vectors are decomposed with the modal basis vectors, each line voltage variation can be determined by applying the TWA technique for all the modal basis vector components as in the single line. In the next section, it will be shown with several practical examples that the generalized TWA technique can be very efficiently exploited in the multicoupled transmission line system.

IV. Verification of the Generalized TWA Technique

Let us consider a simple symmetrical two-coupled line system as shown in Fig. 2. The source resistances are assumed to be 50 Ω (i.e., $R_{s1} = R_{s2} = 50\ \Omega$) and the load capacitances are assumed to be 0.1 pF (i.e., $C_{L1} = C_{L2} = 0.1$ pF). It is assumed that a 3.3-V step input is applied to the line-1 while no signal is applied to the line-2. Then incident wave vector of the system can be represented with the basis vectors by combining (19) with the boundary conditions

$$W_1(s,x) = \frac{1}{2}\left(e^{-\gamma_1 x} + e^{-\gamma_2 x}\right) \quad (20)$$

$$W_1(s,x) = \frac{1}{2}\left(e^{-\gamma_1 x} - e^{-\gamma_2 x}\right) \quad (21)$$

where γ_i^2 $(i = 1, 2)$ is the ith eigenmode. The transmission line parameters for the structure of Fig. 2 are determined by using a commercial field solver [36]. The transmission line parameters are as follows:

$$[R] = \begin{bmatrix} 68.966 & 0 \\ 0 & 68.966 \end{bmatrix}\left[\frac{\Omega}{\mathrm{cm}}\right]$$

$$[L] = \begin{bmatrix} 6.94 & 4.754 \\ 4.754 & 6.94 \end{bmatrix}\left[\frac{\mathrm{nH}}{\mathrm{cm}}\right]$$

$$[C] = \begin{bmatrix} 2.263 & -0.534 \\ -0.534 & 2.263 \end{bmatrix}\left[\frac{\mathrm{pF}}{\mathrm{cm}}\right].$$

TABLE I
Representative Input Switching Patterns for Three-Coupled Lines and the Physical Characteristics Corresponding to Each Switching Pattern

Switching patterns	Physical characteristics of 3-coupled lines
0↑0	Total-capacitance-based delay model in the center line
↓↑↓	The worst case capacitive-delay in the center line
↑↑↑	No coupling-capacitive delay in the center line
↑0↑	The worst case crosstalk noise in the center (quiet) line

Note, the dielectric loss term is neglected. The modal transmission line parameters of the system are calculated by using (15)-(18)

$$[R_m] = \begin{pmatrix} R_{11} & 0 \\ 0 & R_{11} \end{pmatrix} = \begin{bmatrix} 68.966 & 0 \\ 0 & 68.966 \end{bmatrix}\left[\frac{\Omega}{\mathrm{cm}}\right]$$

$$[L_m] = \begin{pmatrix} L_{11}+L_{12} & 0 \\ 0 & L_{11}-L_{12} \end{pmatrix} = \begin{bmatrix} 11.694 & 0 \\ 0 & 2.186 \end{bmatrix}\left[\frac{\mathrm{nH}}{\mathrm{cm}}\right]$$

$$[C_m] = \begin{pmatrix} C_{11}-C_{12} & 0 \\ 0 & C_{11}+C_{12} \end{pmatrix} = \begin{bmatrix} 2.797 & 0 \\ 0 & 1.729 \end{bmatrix}\left[\frac{\mathrm{pF}}{\mathrm{cm}}\right].$$

The modal transmission line parameters corresponding to the first eigenmode are the first diagonal parameters. Similarly, the modal transmission line parameters corresponding to the second eigenmode are the second diagonal parameters. Once the incident waves are completely decoupled into the independent eigenmodes, the TWA technique can be directly employed for each eigenmode. That is, each eigenmode response is approximately represented with three-dominant poles as in (4) and (5) in the frequency domain. Then, the time-domain signal transients are calculated by linear combination of each TWA-based eigenmode response. Note, the signal transient responses in the quiet line (i.e., the responses in the line-2 for the two-coupled lines) are the crosstalk signals. The TWA-based waveforms for the above two coupled lines are compared with SPICE simulation results (using large computationally inefficient arrays of small discrete RLC elements) in Fig. 3. They show excellent agreement in signal waveform and crosstalk noise with SPICE simulations. As was expected, not only does the baseline RC-model inaccurately estimate the signal delay but it underestimates the crosstalk. Thus, in ensuing examples, the RC model is not presented.

In the multicoupled lines, the signal transients are strongly dependent on the input-switching patterns [4]. The input switching patterns for three-coupled lines can be categorized with four typical switching cases as shown in Table I. The signal delay in the center line for the input switching pattern of "$0 \uparrow 0$" (i.e., the center line switches from logic 0 to logic 1 but two outer lines are in a quiet state) is commonly tested for timing verification. However, since signal delay is strongly correlated with input switching patterns, two other switching cases (i.e., "$\downarrow\uparrow\downarrow$" and "$\uparrow\uparrow\uparrow$") have to be investigated for more complete signal timing verification. The worst case signal delay in the center line is for the input switching pattern of "$\downarrow\uparrow\downarrow$" (i.e., the center line switches from logic 0 to logic 1 but two outer lines switch from logic 1 to logic 0). This case presents the slowest signal propagation in the center line. This simulation demonstrates that the coupling capacitances have significant effects on the signal propagation in the center line. In contrast, the signal delay in the center line for the input switching pattern of "$\uparrow\uparrow\uparrow$" (i.e., all the lines switch from logic 0 to logic 1) is the best case delay which means the fastest signal propagation in the center line. In this switching case, the coupling capacitances have no effect on the signal propagation in the center line. Further, since the signals are electromagnetically coupled, an active line may have a substantial effect on an inactive line (i.e., quiet lines). In the first switching case (i.e., "$0 \uparrow 0$"), the center line (i.e., active line) induces a coupled signal in the two outer lines (i.e., crosstalk). However, the worst case crosstalk (i.e., the largest crosstalk in the three-coupled line system) occurs in the center line when the input has the switching pattern of "$\uparrow 0 \uparrow$" (i.e., two outer lines switch from logic 0 to logic 1 but the center line is in the inactive state). Note, the signal transient characteristics of other possible switching cases are within the boundaries of those of the above switching patterns. The aforementioned signal transient characteristics for a three-coupled line system can be efficiently investigated with the generalized TWA technique. The transmission line parameters of Fig. 4 (note, its cross-sectional structure is the same as Fig. 2(b) except for three-coupled signal lines) can be calculated by using a commercial field solver [36],

$$[R] = \mathrm{diag}(68.966)\left[\frac{\Omega}{\mathrm{cm}}\right]$$
$$[L] = \begin{bmatrix} 7.160 & 4.924 & 3.838 \\ 4.924 & 7.010 & 4.924 \\ 3.838 & 4.924 & 7.160 \end{bmatrix}\left[\frac{\mathrm{nH}}{\mathrm{cm}}\right]$$
$$[C] = \begin{bmatrix} 2.225 & -0.522 & -0.042 \\ -0.522 & 2.427 & -0.522 \\ -0.042 & -0.522 & 2.225 \end{bmatrix}\left[\frac{\mathrm{pF}}{\mathrm{cm}}\right].$$

Note, " 0 " indicates no switching, "$\uparrow$" indicates a switching from logic 0 to logic 1, and "$\downarrow$" indicates a switching from logic 1 to logic 0.

With the same procedures as in the previous two-coupled lines example, the TWA-based approximated transient waveforms for the three-coupled line system can be determined. All the source resistances are assumed to be 50 Ω (i.e., $R_{s1} = R_{s2} = R_{s3} = 50\,\Omega$) and all the load capacitances are assumed to be 0.1 pF (i.e., $C_{L1} = C_{L2} = C_{L3} = 0.1$ pF). The TWA-based waveforms and SPICE simulations are compared in Fig. 5 for various switching cases. It is noteworthy that the input-signal switching patterns have substantial effect on both the signal delay and crosstalk. Further, unlike the signal transient characteristics of the single line or RC-modeled lines, those of the inductance-dominant coupled lines are shown to be more complicated nonmonotonic waveshapes contaminated with spurious glitches or spikes. Nevertheless, the generalized TWA-based technique can very efficiently as well as accurately estimate the waveshapes. The signal transients that vary with different source resistances and load capacitances are examined at both near end and far end. As shown in Fig. 6, the TWA-based waveforms show excellent agreement with SPICE simulations. As shown in three-coupled lines, the inductive coupling effect and switching-pattern dependency are too significant to be neglected. What is worse, unlike the capacitive coupling effect, the inductive coupling effect cannot be shielded with

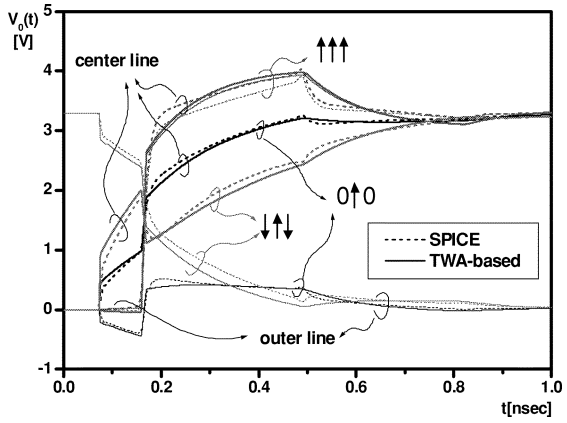

Fig. 5. Transient characteristics in three-coupled line system. Inputs are 3.3-V step. All the source resistances are assumed to be $\boldsymbol{R_{S1} = R_{S2} = R_{S3} = 50\ \Omega}$. All the load capacitances are assumed to be $\boldsymbol{C_{L1} = C_{L2} = C_{L3} = 0.1}$ pF.

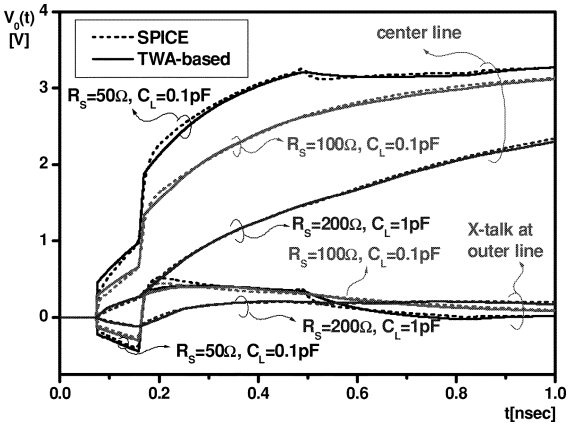

(a)

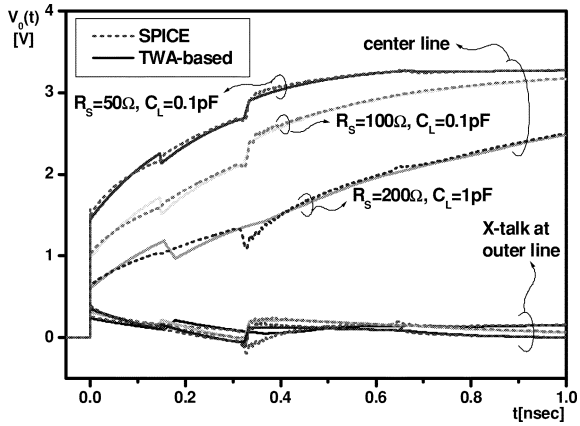

(b)

Fig. 6. The signal transients with various source resistances and capacitances: (a) far end and (b) near end.

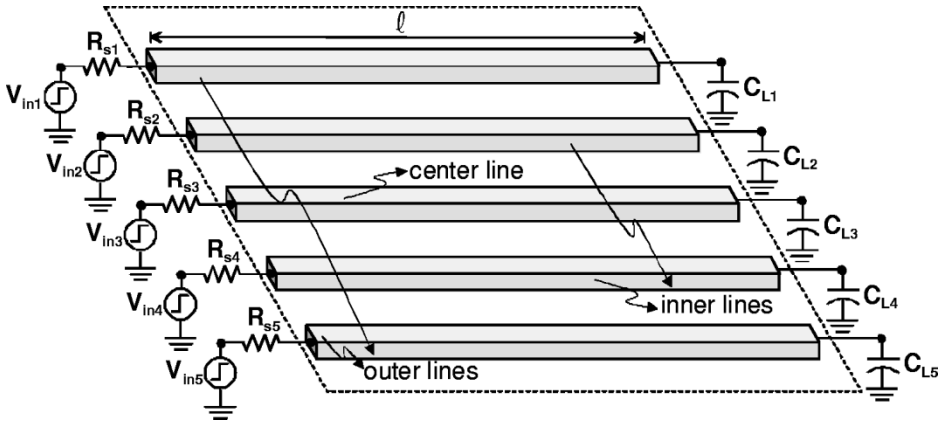

Fig. 7. Five-coupled transmission line system.

TABLE II
REPRESENTATIVE INPUT SWITCHING PATTERNS FOR FIVE-COUPLED LINES AND THE PHYSICAL CHARACTERISTICS CORRESPONDING TO EACH SWITCHING PATTERN

Switching patterns of 5-coupeld lines	Comparable patterns with 3-coupled lines	Physical characteristics of each switching patterns
00↑00	0↑0	Total-capacitance-based delay in the center line
↑↓↑↓↑	↓↑↓	The cross-coupled switching with the center line
↓↑↑↑↓	↑↑↑	The cross-coupled switching with the outer lines
↑↑0↑↑	↑0↑	The worst case crosstalk noise in the center line

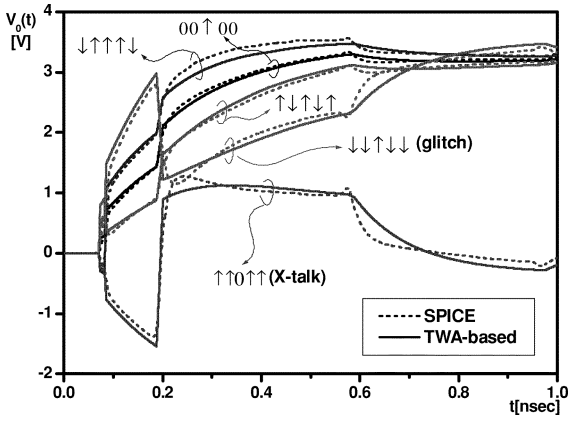

Fig. 8. Transient characteristics in five-coupled line system. Inputs are 3.3-V step. All the source resistances are assumed to be $\boldsymbol{R_{S1} = R_{S2} = R_{S3} = R_{S4} = R_{S5} = 50\,\Omega}$. All the load capacitances are assumed to be $\boldsymbol{C_{L1} = C_{L2} = C_{L3} = C_{L4} = C_{L5} = 0.1}$ pF.

adjacent lines and may have a considerable effect on far-apart lines. Thus, the inductive coupling effects and switching-pattern dependency may render more complicated response waveforms in multicoupled lines with more than three-coupled lines.

In order to investigate the effects in more than three-coupled lines, a five-coupled line system as shown in Fig. 7 is studied. The representative switching patterns for five-coupled lines can be categorized as in three-coupled lines. They are summarized in Table II. The transmission line parameters for the five-coupled lines of Fig. 7 (note, its cross-sectional structure is the same as Fig. 2(b) except for five-coupled signal lines) are determined by using a commercial field solver [36]

$$[R] = \mathrm{diag}\,(68.966)\left[\frac{\Omega}{\mathrm{cm}}\right]$$

$$[L] = \begin{bmatrix} 7.470 & 5.220 & 4.074 & 3.357 & 2.839 \\ 5.220 & 7.257 & 5.115 & 4.028 & 3.357 \\ 4.074 & 5.115 & 7.214 & 5.115 & 4.074 \\ 3.357 & 4.028 & 5.115 & 7.257 & 5.220 \\ 2.839 & 3.357 & 4.074 & 5.220 & 7.470 \end{bmatrix} \left[\frac{\mathrm{nH}}{\mathrm{cm}}\right]$$

$$[C] = \begin{bmatrix} 2.227 & -0.522 & -0.036 & -0.016 & -0.010 \\ -0.522 & 2.432 & -0.514 & -0.032 & -0.016 \\ -0.036 & -0.514 & 1.327 & -0.514 & -0.036 \\ -0.016 & -0.032 & -0.514 & 2.432 & -0.522 \\ -0.010 & -0.016 & -0.036 & -0.522 & 2.227 \end{bmatrix} \left[\frac{\mathrm{pF}}{\mathrm{cm}}\right].$$

In Fig. 7, all the source resistances are assumed to be 50 Ω (i.e., $R_{s1} = R_{s2} = R_{s3} = R_{s4} = R_{s5} = 50\,\Omega$) and all the load capacitances are assumed to be 0.1 pF (i.e., $C_{L1} = C_{L2} = C_{L3} = C_{L4} = C_{L5} = 0.1$ pF). The generalized TWA-based waveforms for the five-coupled line system are compared with SPICE simulation in Fig. 8. Except for the input switching patterns of "↑↑↑↑↑" and "00 ↑ 00 ", the signal transients in the center line for the cross-coupled switching cases show large distortions due to inductive effect. Further, it was shown in Fig. 9 that the signal distortions (spurious glitches) and crosstalk due to the inductive effects in the five-coupled line system are more prominent and produce more complicated waveshapes than those of the three-coupled line system. Thus, in high-speed VLSI circuit designs, the inductive effects cannot be neglected in the future. Further, since switching patterns have a substantial effect on the signal transient characteristics, they have to be taken into account for the signal integrity verification of the VLSI circuit designs. The generalized TWA-based technique provides an excellent waveshape replica of SPICE simulations even in the multicoupled lines more than three-coupled lines. The numerical data for various cases are summarized in Tables III and IV.

V. CONCLUSION

A generalized TWA technique is developed which can be very accurately as well as efficiently employed for a transient signal

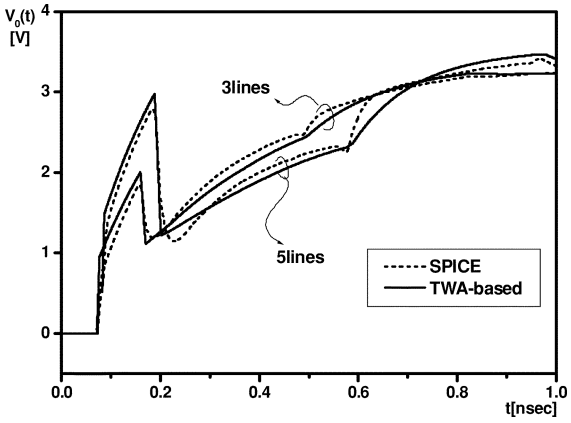

(a)

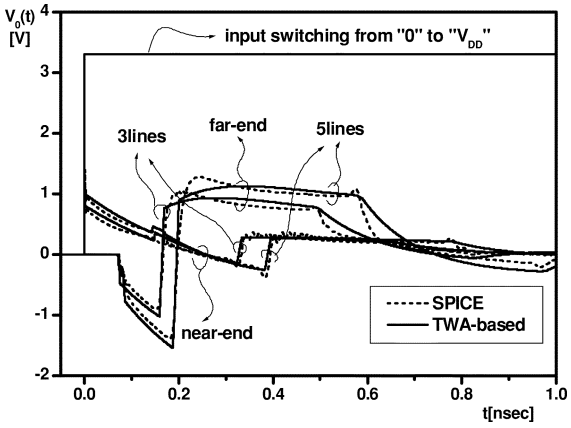

(b)

Fig. 9. Transient signal comparisons for three-coupled and five-coupled line systems. While the three-coupled lines have the switching pattern of ($\downarrow\uparrow\ \downarrow$), the five-coupled lines have the switching pattern of ($\downarrow\downarrow\uparrow\ \downarrow\downarrow$). All the source resistances are assumed to be $\boldsymbol{R}_{S1} = \boldsymbol{R}_{S2} = \boldsymbol{R}_{S3} = \boldsymbol{R}_{S4} = \boldsymbol{R}_{S5} = \mathbf{50}\ \boldsymbol{\Omega}$. All the load capacitances are assumed to be $\boldsymbol{C}_{L1} = \boldsymbol{C}_{L2} = \boldsymbol{C}_{L3} = \boldsymbol{C}_{L4} = \boldsymbol{C}_{L5} = \mathbf{0.1}$ pF. (a) Center line signal transients at far end. (b) The worst case crosstalk noises at the near end and far end.

TABLE III
PEAK CROSSTALK NOISES IN MULTICOUPLED LINES

Line #	Near-end[V]		Far-end[V]	
	TWA	SPICE	TWA	SPICE
2lines($\uparrow$0)	0.44	0.45	0.73	0.63
3lines($\uparrow$0$\uparrow$)	0.81	0.81	1.03	1.01
5lines($\uparrow\uparrow$0$\uparrow\uparrow$)	1.00	1.02	1.55	1.39

characterization in a multicoupled transmission line system. The multicoupled lines are decoupled into isolated basis vectors by using the well-known modal analysis technique. The voltage signal variations in all the lines can be very efficiently determined with the linear combination of the decoupled basis vector responses. That is, applying the single-line-based TWA technique to the decoupled eigenmodes, the signal integrity of muticoupled lines such as signal delay, overshoots, undershoots, and crosstalk can be very accurately as well as efficiently investigated. Since the technique can provide the close form solution of the signal waveform, it can be very usefully employed in the signal integrity verification of high-speed/high-density VLSI circuit designs.

TABLE IV
50% DELAYS FOR VARIOUS SWITCHING CONDITIONS IN MULTICOUPLED LINES

Line #	Switching patterns	50% Delay [psec]							
		1mm		2mm		5mm		10mm	
		TWA	SPICE	TWA	SPICE	TWA	SPICE	TWA	SPICE
2lines	0$\uparrow$	16.8	18.0	31.4	32.4	75.4	76.6	148.7	152.2
3lines	$\uparrow\uparrow\uparrow$	21.6	21.6	37.6	37.8	85.4	86.4	165.8	167.6
	0$\uparrow$0	17.4	19.2	33.8	35.6	83.6	85.2	167.0	168.8
	$\downarrow\uparrow\downarrow$	9.6	10.8	17.0	19.0	108.2	113.6	273.8	258.4
5lines	$\uparrow\uparrow\uparrow\uparrow\uparrow$	25.6	25.4	44.4	44.4	100.8	101.6	195.2	196.8
	00$\uparrow$00	13.2	17.6	26.2	32.6	85.2	92.6	192.0	193.4
	$\downarrow\downarrow\uparrow\downarrow\downarrow$	9.8	10.4	18.0	18.8	130.2	134.4	322.4	313.0

REFERENCES

[1] "National Technology Roadmap Semiconductors Technology Needs," SIA, 1997.

[2] D. W. Bailey and B. J. Benschneider, "Clocking design and analysis for a 600-MHz alpha microprocessor," *IEEE J. Solid-State Circuits*, vol. 33, pp. 1627–1633, Nov. 1998.

[3] S. Lin and E. Kuh, "Transient simulation of lossy interconnects based on the recursive convolution formulation," *IEEE Trans. Circuit Syst. I*, vol. 39, pp. 879–892, Nov. 1992.

[4] A. D. Deutsch *et al.*, "When are transmission-line effects important for on-chip interconnections ?," *IEEE Trans. Microwave Theory Tech.*, vol. 45, pp. 1836–1997, Oct. 1997.

[5] Y. Massoud and Y. Ismail, "Grasping the impact of on-chip inductance," *IEEE Circuits and Devices*, vol. 17, pp. 14–21, July 2001.

[6] Y. I. Ismail, E. G. Friedman, and J. L. Neves, "Figure of merit to characterize the importance of on-chip inductance," *Proc. ACM/IEEE Design Automation Conf.*, pp. 560–565, 1998.

[7] A. D. Deutsch *et al.*, "Modeling and characterization of long on-chip interconnections for high-performance microprocessors," *IBM J. Res. Develop.*, vol. 39, no. 5, pp. 537–566, Sep. 1995.

[8] C. W. Ho, "Theory and computer-aided analysis of lossless transmission lines," *IBM J. Res. Develop.*, vol. 17, no. 5, pp. 249–255, May 1973.

[9] A. J. Gruodis, "Transient analysis of uniform resistive transmission lines in a homogeneous medium," *IBM J. Res. Develop.*, vol. 23, no. 6, pp. 537–566, Nov. 1979.

[10] A. J. Gruodis and C. S. Chang, "Coupled lossy transmission line characterization and simulation," *IBM J. Res. Develop.*, vol. 25, no. 1, pp. 25–41, Jan. 1981.

[11] F.-Y. Chang, "Transient analysis of lossless coupled transmission lines in a nonhomogeneous dielectric medium," *IEEE Trans. Microwave Theory Tech.*, vol. 18, pp. 616–626, Sept. 1970.

[12] J. S. Roychowdhury, A. R. Newton, and D. O. Pederson, "An impulse-response-based linear time complexity algorithms for lossy interconnect simulation," in *Proc. ICCAD*, 1991, pp. 62–65.

[13] F.-Y. Chang, "Waveform relaxation analysis of RLCG transmission lines," *IEEE Trans. Circuit Syst.*, vol. 37, pp. 1394–1415, Nov. 1990.

[14] ——, "Transient simulation of nonuniform coupled lossy transmission lines characterized with frequency-dependent parameters-Part I; Waveform relaxation analysis," *IEEE Trans. Circuit Syst. I*, vol. 39, pp. 585–603, Aug. 1992.

[15] ——, "Transient simulation of nonuniform coupled lossy transmission lines characterized with frequency-dependent parameters-Part II; Discrete time analysis," *IEEE Trans. Circuit Syst. I*, vol. 39, pp. 907–927, Nov. 1992.

[16] A. R. Djordjevi'c, T. K. Sarkar, and R. F. Harrington, "Analysis of lossy transmission lines with arbitrary nonlinear terminal networks," *IEEE Trans. Microwave Theory Tech.*, vol. MTT-34, pp. 660–666, June 1986.

[17] D. Winkestein, M. B. Steer, and R. Pomerleau, "Simulation of arbitrary transmission line network with nonlinear terminations," *IEEE Trans. Circuit Syst.*, vol. 38, pp. 418–412, Apr. 1991.
[18] R. J. Antinone and G. W. Brown, "The modeling of resistive interconnects for integrated circuits," *IEEE J. Solid-State Circuits*, vol. SC-18, pp. 200–203, Apr. 1983.
[19] L. T. Pillage and R. A. Rohrer, "Asymptotic waveform evaluation for timing analysis," *IEEE Trans. Computer-Aided Design*, vol. 9, pp. 352–368, Apr. 1990.
[20] L. M. Silveira, I. M. Elfadel, J. K. White, M. Chilukuri, and K. S. Kundert, "Efficient frequency-domain modeling and circuit simulation of transmission lines," *IEEE Trans. Comp., Packag., Manufact., Technol. B*, vol. 17, no. 4, pp. 505–513, Nov. 1994.
[21] D. B. Kuznetsov and J. E. Schutt-Aine, "Optimal transient simulation of transmission lines," *IEEE Trans. Circuit Syst. I*, vol. 43, pp. 110–121, Feb. 1996.
[22] L. M. Silveira, M. Kamon, and J. White, "Efficient reduced-order modeling of frequency-dependent coupling inductances associated with 3-D interconnect structures," *IEEE Trans. Comput., Packaging, Manuf., Technol. B*, vol. 19, pp. 283–288, May 1996.
[23] R. W. Freund and P. Feldmann, "Reduced-order modeling of large linear subcircuits via a block lanczos algorithm," in *Proc. Design Automation Conf.*, June 1995, pp. 474–479.
[24] D. L. Boley, "Krylov space methods on state-space control models," *J. Circuits, Syst., Signal Processing*, vol. 13, pp. 733–758, May 1994.
[25] A. Idabasioglu, M. Celik, and T. L. Pillage, "PRIMA: Passive reduced-order interconnect macromodeling algorithm," *IEEE Trans. Computer-Aided Design*, pp. 645–654, Aug. 1998.
[26] R. W. Freund and P. Feldmann, "Reduced-order modeling of large passive linear circuits by means of the SyPVL algorithm," *Proc. ACM/IEEE Int. Conf. Computer-Aided Design*, pp. 280–287, Nov. 1996.
[27] B. Young, *Digital Signal Integrity*. Upper Saddle River, NJ: Prentice-Hall, 2001, pp. 1–54.
[28] Y. I. Ismail, E. G. Friedman, and J. L. Neves, "Equivalent elmore delay for RLC trees," *IEEE Trans. Computer-Aided Design*, vol. 19, pp. 83–97, Jan. 2000.
[29] Y. C. Cao *et al.*, "A new analytical delay and noise model for on-chip RLC interconnect," in *Proc. Int. Electronic Device Meeting*, 2000, pp. 823–826.
[30] J. A. Davis and J. D. Meindl, "Compact distributed RLC interconnect models-Part II: Coupled line transient expressions and peak crosstalk in multi-level networks," *IEEE Trans. Electron. Devices*, vol. 47, pp. 2078–2087, Nov. 2000.
[31] L. Yin and L. He, "An efficient analytical model of coupled on-chip RLC interconnects," in *Proc. Asia South Pacific Design Automation Conf.*, 2001, pp. 385–390.
[32] Y. Eo, J. Shim, and W. R. Eisenstadt, "A traveling-wave-based waveform approximation technique for the timing verification of single transmission lines," *IEEE Trans. Computer-Aided Design*, vol. 21, pp. 723–730, June 2002.
[33] H. You and M. Soma, "Crosstalk analysis of interconnect lines and packages in high speed integrated circuits," *IEEE Trans. Circuit Syst.*, vol. 37, pp. 1019–1026, Aug. 1990.
[34] L. T. Hwang, D. Nayak, I. Turlik, and A. Resiman, "Thin film pulse propagation analysis using frequency techniques," *IEEE Trans. Comp., Hybrids, Manufact. Technol.*, vol. 14, pp. 192–198, Mar. 1991.
[35] K. D. Granzow, *Digital Transmission Lines*. New York: Oxford Univ. Press, 1998, pp. 133–168.
[36] *Maxwell Q2D/Q3D Parameter Extractor User's Reference*, Ansoft Corp., Pittsburgh, PA, 1999.

Implementation of a Comprehensive and Robust MOSFET Model in Cadence SPICE for ESD Applications

X. F. Gao, J. J. Liou, J. Bernier, G. Croft, and A. Ortiz-Conde

***Abstract*—Electrostatic discharge (ESD) is a critical reliability concern for microchips. This paper presents a comprehensive computer-aided design tool for ESD applications. Specifically, the authors develop an improved and robust MOS model and implement such a model into the industry standard Cadence SPICE for ESD circuit simulation. The key components relevant to ESD in the MOS model are studied and the implementation procedure is discussed. Experimental data measured from the human body model tester are included in support of the model.**

***Index Terms*—Electrostatic discharge, modeling, MOSFET, SPICE.**

I. Introduction

Electrostatic discharge (ESD) is an event that transfers a finite amount of charge between two objects at different potentials [1]. A frequently occurred ESD event is the human body model (HBM), where the two different objects involved are charged human body and microchip. To prevent microchips from being damaged by the ESD event, ESD protection circuits (i.e., supply clamps) have frequently been used. A typical ESD protection circuit consists of a capacitor, a resistor, and an n-channel MOSFET [2], as shown in Fig. 1. When the microchip (i.e., circuit core) being protected is subjected to an ESD stress, the ESD pulse will be fed simultaneously to the external capacitor C and drain terminal of the MOSFET in the ESD protection circuit. Such a pulse, which has a very high voltage (a few hundred to couple of thousand volts), will give rise to a voltage drop in the external resistor R and therefore will turn on the MOSFET within a very short period of time. On the other hand, the ESD pulse applied to the drain terminal will result in a large electric field in the reverse biased drain junction region. This electric field can cause significant impact ionization and give rise to a substantial flow of impact generated holes (i.e., substrate current $I_{\rm sub}$), traveling from the channel region near the drain junction to the body terminal via the substrate region of MOSFET. When the voltage drop in the substrate region, which is the product of $I_{\rm sub}$ and the substrate resistance $R_{\rm sub}$, is beyond 0.7 V, the emitter-base junction of the parasitic bipolar transistor (BJT) in the MOSFET is turned on and the MOSFET operates in the so-called snapback region. The equivalent circuit of the MOSFET in snapback operation is shown in Fig. 2, which consists of the normal MOSFET, parasitic BJT, $R_{\rm sub}$, and source of impact-generated hole current $I_{\rm gen}$. The total current passing through the drain terminal is I_{DT}, which includes $I_{\rm gen}$, the drain current I_{ds}, and the collector current I_C of the parasitic BJT.

Substrate resistance $R_{\rm sub}$ plays an important role in determining the turn-on mechanism of the parasitic BJT. This resistance is influenced

Manuscript received November 13, 2001; revised February 27, 2002. X. F. Gao and J. J. Liou were supported in part by the Semiconductor Research Corporation and Intersil Corporation, Palm Bay, FL. This paper was recommended by Associate Editor Z. Yu.

X. F. Gao and J. J. Liou are with the School of Electrical Engineering and Computer Science, University of Central Florida, Orlando, FL 32816 USA (e-mail: liou@pegasus.cc.ucf.edu).

J. Bernier is with the Reliability Engineering Department, Intersil Corporation, Palm Bay, FL 32905 USA.

G. Croft is with the Technology Development Department, Intersil Corporation, Palm Bay, FL 32905 USA.

A. Ortiz-Conde is with the Electronics Engineering Department, University Simon Bolivar, Caracas, Venezuela.

Digital Object Identifier 10.1109/TCAD.2002.804379